

# A Scanning Line Source for Simultaneous Emission and Transmission Measurements in SPECT

Patrick Tan, Dale L. Bailey, Steven R. Meikle, Stefan Eberl, Roger R. Fulton and Brian F. Hutton

*Department of Nuclear Medicine, Royal Prince Alfred Hospital; and Centre for Biomedical Engineering, University of New South Wales, Sydney, Australia*

A scanning collimated line source for simultaneously acquiring emission and transmission data from a gamma camera has been developed. The line source is microprocessor-controlled and incorporates hardware to electronically window the spatial gamma camera signals in order to separate the emission signals of the subject from transmission signals from the line source. The device improves upon the previously described emission-transmission scanning technique using a flood source in three ways: (1) it overcomes the limitation that the transmission radionuclide must have a lower energy than the emission radionuclide; (2) it provides narrow-beam (scatter free) attenuation measurements of the subject being examined; and (3) it reduces the radiation exposure to staff. Attenuation coefficients for an elliptical water-filled phantom were measured to be  $\mu = 0.15 \pm 0.01 \text{ cm}^{-1}$ . The technique has been validated in phantom and human studies using a range of radionuclide combinations and imaging geometries and gives equivalent results using separate and simultaneous acquisitions.

*J Nucl Med* 1993; 34:1752-1760

Single photon emission computed tomography (SPECT) is used extensively in diagnostic nuclear medicine for qualitatively assessing radiopharmaceutical distributions in vivo. A major limitation on both qualitative and quantitative SPECT is inaccuracy due to incorrect compensation for attenuated photons. Although no analytically exact solution for the problem of photon attenuation has been described, numerous algorithms for attenuation correction have been reported (1-3) which achieve a high degree of quantitative accuracy when combined with transmission measurements (4-11). The use of transmission measurements to improve the accuracy of scatter correction has also been suggested (12,13). These developments indicate that the quantitative potential of SPECT may well be realizable when combined with appropriate correction tech-

niques. However, for transmission-based quantitative SPECT to be useful in the clinical department, it must be possible to acquire both emission and transmission data within a practical time frame.

In a previous report from this department, a technique was described for simultaneously acquiring emission and transmission data using a sheet (flood) transmission source of lower photon energy than the emission source (14). This approach suffers from several drawbacks. First, significant cross-contamination of the emission and transmission data occurs, requiring postacquisition processing to remove the cross-talk, which may affect the accuracy of the measurements. Second, the use of an uncollimated sheet source results in broad-beam attenuation coefficients ( $\mu$ ) since transmission scatter is included in the measurement. This is inappropriate for attenuation correction of emission data that has been scatter corrected. Third, it is highly desirable to use a transmission source with the same photon energy as the emission source. However, the flood source method requires that the two radionuclides be separable by pulse-height analysis. Despite these limitations, the method was favorably reviewed (15) as a practical method for improving the accuracy of SPECT measurements. The flood source method has since been improved by collimating the source, and extended to allow the use of a transmission source with higher photon energy than the emission source, with application in  $^{201}\text{Tl}$  myocardial perfusion imaging (16). However, the problems of cross-talk and restrictions on the choice of radionuclides remain.

This paper reports on an improvement in the simultaneous emission-transmission technique which has been developed to overcome the limitations of the flood source method. A scanning line source has been designed and implemented which uses a combination of physical and electronic collimation. This technique greatly reduces scatter compared to the previous method. It also overcomes the restrictions on the choice of emission and transmission radionuclides. For example, it is possible to acquire a transmission scan using the same radionuclide (or one with similar photon energy) as the emission radionuclide with minimal increase in scanning time over a conventional

Received Nov. 19, 1992; revision accepted June 17, 1993.  
For correspondence and reprints contact: Dale L. Bailey, Dept. of Nuclear Medicine, Royal Prince Alfred Hospital, Camperdown NSW 2050, Australia.

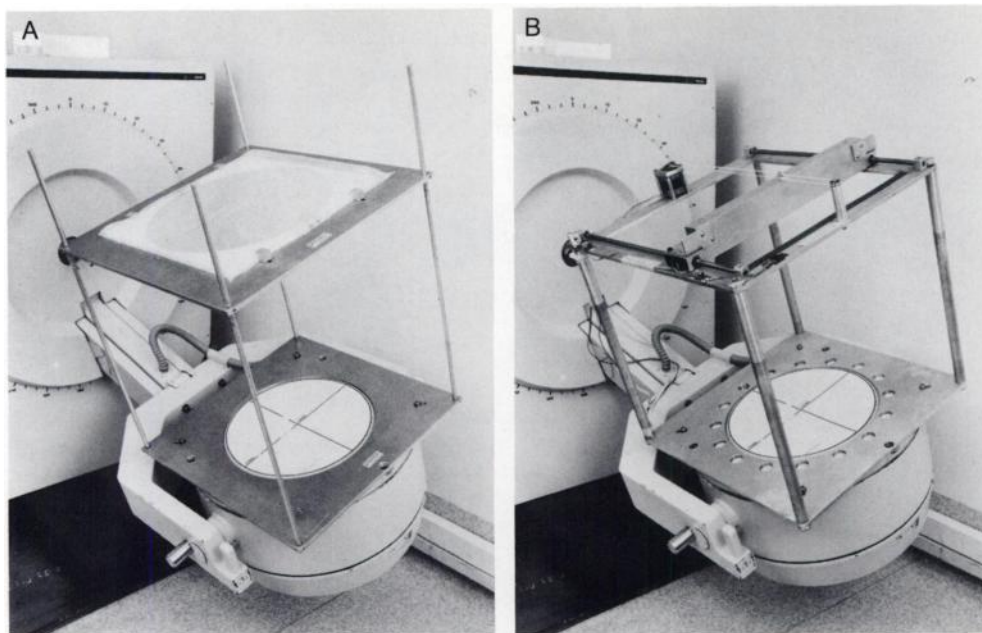


**FIGURE 1.** (A) The previously published method for simultaneous emission-transmission tomography used a sheet source of  $^{163}\text{Gd}$  mounted on the gamma camera. (B) The scanning transmission line source is mounted on the gamma camera in a similar manner to the previous sheet source method. The stepper motor is located at the far end of the frame. The lead shielding in the resting position can be seen built into the support frame at the end closest to the viewer.

SPECT study. The source has been primarily designed with SPECT acquisitions in mind, but may be applied in planar imaging, or in quality control procedures (17). The device has been implemented on a commercial rotating gamma camera/computer system and validated in both phantom studies and human subjects.

## MATERIALS AND METHODS

### Design

The line source is mounted onto the gamma camera detector head in a similar manner to the flood source technique described previously (Fig. 1). In its zero position, the line source is retracted behind lead shielding built into the housing, thereby rendering it safe to handle when not in use. The radionuclide source is sealed in a cylindrical perspex tube with a 1-mm internal diameter. The line source is collimated with lead employing a dual slit design (Fig. 2). The dual slit design was utilized to provide a narrow beam of gamma rays while minimizing the weight of the device, enabling it to be mounted on a conventional gamma camera head with little modification. The effective collimator length is 50 mm with a 1-mm aperture. The minimum thickness of lead surrounding the line source is equivalent to 3 tenth-value layers for 140 keV photons (approximately 7 mm). The lead source holder is encased in

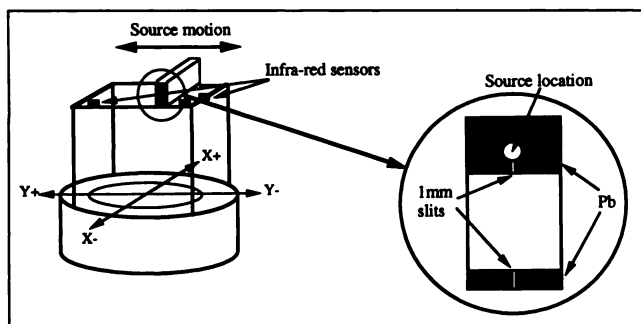


**FIGURE 2.** Detail of the line source collimation. The minimum thickness of lead is equivalent to three tenth-value layers for  $^{99\text{m}}\text{Tc}$  photons.

aluminum. The collimation was designed so that the area irradiated by the source is less than 10% of the field of view in the y-dimension of the gamma camera, leaving the remainder of the field of view available for simultaneously acquiring emission events. This translates to approximately a 44-mm region on a conventional large field of view gamma camera with the line source at 0.75 m from the collimator. A similar photon flux to the flood source previously used, which contained approximately 1.5 GBq (40 mCi), is achieved by filling the line source container with a total activity of approximately 6 GBq (162 mCi). The collimation also reduces radiation exposure to staff from the transmission source. This was estimated to be less than  $0.5 \mu\text{Gy}$  for a 30-min exposure using a hand-held survey monitor at a distance of 1 m from the source which contained approximately 5 GBq at the time of the measurement. This compares with approximately  $100 \mu\text{Gy}$  using an uncollimated flood source containing 1.5 GBq.

The frame which supports the line source attaches directly to the edge of the collimator and positions the line source 0.75 m from the collimator. At this distance, the line source and frame does not interfere with patient positioning or compromise patient-to-detector distance for optimal resolution. Extra counter-weights have been attached to the gantry to support the additional weight of the line source ( $\sim 10 \text{ kg}$ ).

There are two main functional components to the electronic hardware: the line source motion controller and the electronic (spatial) collimation circuit. These are controlled by a microprocessor containing all the run-time functions of the high level FORTH language in a ROM kernel (R65F12, Rockwell International Corporation, El Segundo, CA). In the current implementation, the application program is loaded from another computer (a PC) via a serial port and stored in RAM.

### Line Source Motion Control

The line source traverses the field-of-view in the Y-direction so that its motion is equally affected by gravity at all angles as the detector rotates about the subject. A functional diagram of the line source control circuit is shown in Figure 3. A bi-directional stepper motor drives the transmission line source. The computer controls the direction (forward or reverse) and stepping rate (ve-

locity) of the motor. Three infrared sensors enable the computer to keep track of the position of the line source. One of the sensors detects the origin or resting position for the zero reference. Another sensor detects the starting position and the third sensor, which is located a known distance from the start sensor, detects the end of a traverse for internal calibration. The gamma camera gantry signals (rotate/start/stop) from the acquisition computer are monitored allowing the line source microprocessor to synchronize the start of each pass with the beginning of each projection angle, including rotation and settling time of the gamma camera.

### Electronic Collimation

The electronic (spatial) collimation is achieved by monitoring Y-position signals and windowing the corresponding Z-signals (unblank) from the gamma camera. There are two distinct processes: (1) an electronic window which moves in synchrony with the known position of the line source and (2) the Z-windows, which determine whether a Z-pulse is accepted or not, depending on the Y-location of the event and whether it is a transmission event ( $Z_a$ ) or an emission event ( $Z_b$ ).

The electronic window must move in step with the transmission line source as it moves in the Y-direction. The moving electronic window has an upper limit,  $Y_u$ , and a lower limit,  $Y_l$ .  $Y_l$  and the window width,  $Y_w$ , are generated by separate digital-to-analog converters.  $Y_u$  is obtained by summing  $Y_l$  and  $Y_w$ . At present, an operating window width of 44 mm (7 pixels wide in a 64 pixel field of 400 mm) is used, but this may be varied.  $Y_l$  and  $Y_u$  are incremented and decremented respectively under the control of the computer which registers the number of steps taken by the line source as it moves. An initial calibration pass is performed to measure the travel distance and start and stop positions. Any DC offset mismatch detected can be corrected in software. Once calibrated, software ensures that the window moves in step with the line source.

In order to determine if a particular Z signal is a transmission or emission event, Y pulses from the gamma camera are continuously compared with  $Y_l$  and  $Y_u$  through a comparator. If the result of the comparison shows Y to be between the values of  $Y_l$  and  $Y_u$  it is assumed to be a transmission event. The emission window

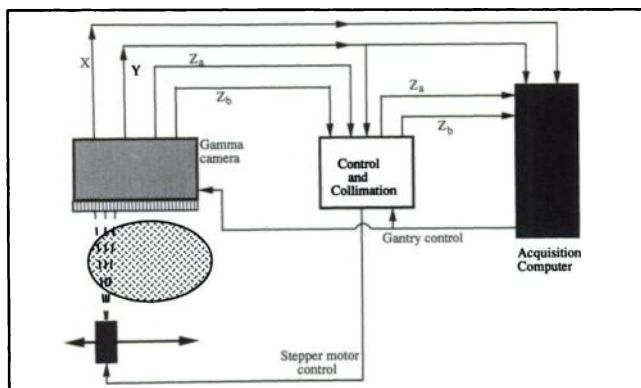


**FIGURE 3.** The line source motion controller and electronic collimation is introduced between the gamma camera and acquisition computer. The Y-signals from the camera are monitored to determine if an event falls within the electronic (spatial) window corresponding to the known position of the line source. The Z-signals (unblank) are accordingly sent to either the transmission ( $Z_a$ ) or emission ( $Z_b$ ) acquisition matrix. The controller also monitors the gantry control signals to ensure that the line source is synchronized with gantry rotation.

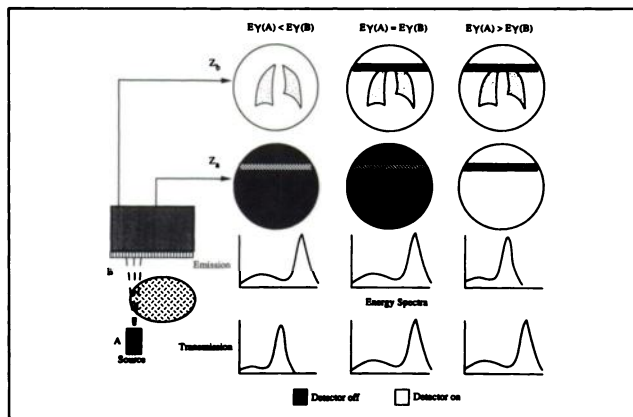


**FIGURE 4.** Schematic representation of the operating modes of the scanning line source for simultaneous emission-transmission tomography. When the transmission radionuclide energy ( $E_y(A)$ ) is less than the emission radionuclide energy ( $E_y(B)$ ) only the transmission data are windowed, restricting recorded transmission events to those occurring within the line source window. The transmission frame is effectively turned "off" for the rest of the field-of-view. When  $E_y(A) = E_y(B)$  both datasets are windowed (emission turned "off" at the location of the line source and transmission turned "on"). When  $E_y(A) > E_y(B)$  only the emission data requires windowing. As the emission data are windowed in the latter two cases, the acquisition time needs to be increased by an amount given by the ratio of the line source window width to the total field of view (~10%) to maintain the same total acquired emission events.

( $W_e$ ) then closes a logic gate to stop the signal from being accepted in the emission frame, and the transmission window ( $W_t$ ) opens a logic gate to enable the event to be accepted. The reverse is the case if the result of the comparison shows Y to be outside the values of  $Y_l$  and  $Y_u$ . Each window may be independently enabled or disabled.

### Implementation

It is possible with the line source and electronic collimation to use any combination of emission and transmission radionuclides (Fig. 4). In the case where the transmission radionuclide has lower photon energy than the emission radionuclide (e.g.,  $^{153}\text{Gd}$  and  $^{99\text{m}}\text{Tc}$  for transmission and emission, respectively), the  $W_t$  window accepts all events that are detected within the region corresponding to the line source and excludes events which are detected outside this region from the transmission frame. This eliminates those scattered emission photons which lose sufficient energy to fall within the transmission photopeak but which are detected outside the spatial window. This does not, however, remove those scattered emission events which are detected inside the spatial window and which fall into the transmission photopeak. These can be corrected using the same convolution-subtraction technique as in the previous emission-transmission method (18), but the down-scatter in this case has been reduced by around 90% and accounts for less than 5% of total recorded events. This is because of the limited time the acceptance window is activated at any position as the line source traverses the field of view. It is not necessary to activate the emission window ( $W_e$ ) in this case as the lower photon energy of the transmission source precludes it from being recorded in the emission window; that is, all events that are within the emission photopeak are accepted as emission events. Therefore, in this configuration, a simultaneous emission-transmission scan can be performed with no increase in scanning time.

For the case where the transmission radionuclide has higher photon energy than the emission radionuclide (e.g.,  $^{99m}\text{Tc}$  and  $^{201}\text{Tl}$ , respectively), only the emission window ( $W_e$ ) need be applied, the opposite of the above situation. As the line source is well collimated it is only necessary to restrict transmission photons from the emission pulse-height channel at the location of the source. Conversely, because the emission photon energy is lower than the transmission photon energy, it is not necessary to electronically window the transmission data to exclude emission photons. This combination of physical and electronic collimation eliminates scattered transmission events recorded within the spatial window which lose sufficient energy to fall into the emission photopeak.

Finally, for the case where transmission and emission radionuclides have the same photon energy, both  $W_e$  and  $W_t$  windows are applied. Since the line source is well collimated, the transmission flux outside the spatial window is low and the number of transmission photons which scatter into this region without losing appreciable energy (sufficient to prevent detection) is expected to be negligibly small. Although emission events occurring within the spatial window cannot be excluded by energy discrimination, the fraction of the field of view activated by the spatial window during each traverse is known and therefore the contribution of emission counts to the window can be easily calculated and a simple subtraction of images performed.

In the latter two cases where the emission window ( $W_e$ ) is applied, effectively turning the emission frame off in the region of the line source, the scanning time must be increased to maintain the same number of total acquired emission counts. This increase is equal to the fraction of the field of view occupied by the electronic window, and is approximately 10% in the present implementation.

### Validation

Experiments were performed to assess the physical performance of the scanning line source using a standard large field of view gamma camera (Philips Gamma Diagnost A, Hamburg, Germany) and a stand-alone acquisition and processing computer (PDP-11 with NCV-11C gamma camera interface, Digital Equipment Corporation, Maynard, MA). All results quoted are for this configuration using a low-energy, general-purpose (LEGP) collimator, with  $^{99m}\text{Tc}$  for both the emission and transmission sources, unless otherwise stated.

### Line Spread Function

The line spread function of the transmission source was measured both in air and through 10 cm of tissue-equivalent material. Data were acquired in a  $256 \times 256$  matrix and profiles orthogonal to the line source generated. These were subsequently fitted with a Gaussian function and full widths at half and tenth maxima calculated. These data were also used to assess the contribution of scattered transmission events outside the 7 pixel wide spatial window.

### Uniformity

The uniformity of the gamma camera using the line source was studied as a general measure of performance as there are potentially a number of factors which could influence the quality of the data when used in simultaneous mode. These include: (1) mispositioning of events; (2) spatial variation in countrate with rotation angle (due to sagging or unbalanced torque on the camera head) (3) variations in scanning velocity and (4) high local count rates outside the subject's body which may cause mispositioning of

events in the transmission window. To examine these effects, acquisitions were performed with a  $^{57}\text{Co}$  sheet source (Amer-sham, UK; guaranteed uniformity >97%) and the line source. High count images (50 M cts) of the flood source were acquired both with and without the line source present to examine whether there was any degradation due to the presence of the source and the electronic windowing. For this the line source was operated in a static, multi-pass planar mode. In addition, a SPECT study of the line source alone was acquired in simultaneous mode with windowing of both the transmission and emission events. These frames were considered separately (for reproducibility) and added together (for high count measurements) and compared with static acquisitions for the same total counts. NEMA (19) uniformity figures (integral and differential uniformity for the central field-of-view) and a uniformity index (20) were used as measures of flood field uniformity.

### Reconstruction of Attenuation Coefficients

To measure the attenuation coefficients obtained with the line source, a tomographic transmission study of an elliptical water-filled cylinder (dimensions major axis: 28.5 cm, minor axis: 20 cm, length: 30 cm) was performed: 64 images in a  $64 \times 64$  matrix were acquired over a  $360^\circ$  orbit at 20 sec per projection angle. A blank scan (transmission scan without the object in the field of view) was also acquired. Projections of attenuation coefficients were formed by taking the natural logarithm of the blank-to-transmission scan ratio at each angle and reconstructed using filtered backprojection with a Shepp-Logan window with critical frequency equal to the Nyquist frequency. The study was repeated using an uncollimated flood source and the reconstructed  $\mu$  values obtained by the two methods were compared by assigning regions of interest (ROI) to the central portion of the image and by examining count profiles through the reconstructed images.

### Simultaneous Acquisition

Phantom studies were performed using different combinations of emission and transmission radionuclides to compare SPECT measurements in simultaneous and separate modes for each imaging situation. All studies were performed with  $360^\circ$  acquisition and 40 sec per angle. Prior to adding activity, transmission studies of an elliptical water-filled phantom were performed using  $^{99m}\text{Tc}$  and  $^{153}\text{Gd}$  as the transmission sources. The phantom was then filled with a uniform concentration of approximately  $10 \text{ kBq} \cdot \text{ml}^{-1}$  of  $^{99m}\text{Tc}$  and an emission (only) study was acquired. Simultaneous emission-transmission studies were then carried out using  $^{99m}\text{Tc}$  and  $^{153}\text{Gd}$  as the transmission source. After allowing the activity to decay over a 72-hr period, the phantom was filled with a uniform concentration of approximately  $10 \text{ kBq} \cdot \text{ml}^{-1}$  of  $^{201}\text{Tl}$ . Separate and simultaneous studies were performed on the phantom containing  $^{201}\text{Tl}$ , using only  $^{153}\text{Gd}$  as the transmission source in this instance. These studies represent the three imaging situations of interest: (1) emission energy lower than transmission energy ( $^{201}\text{Tl}/^{153}\text{Gd}$ ); (2) emission energy equal to transmission energy ( $^{99m}\text{Tc}/^{99m}\text{Tc}$ ); and (3) emission energy higher than transmission energy ( $^{99m}\text{Tc}/^{153}\text{Gd}$ ).

For the simultaneous  $^{99m}\text{Tc}/^{153}\text{Gd}$  study, downscatter from the  $^{99m}\text{Tc}$  emission window into the  $^{153}\text{Gd}$  transmission window was estimated by convolution of the  $^{99m}\text{Tc}$  image with a bi-exponential function of the form  $Ae^{-br} + Ce^{-dr}$  using  $A = 18$ ,  $b = 1.15 \text{ cm}^{-1}$ ,  $C = 1$  and  $d = 0.1 \text{ cm}^{-1}$ . This method is the same as that used previously with the flood source (14, 18), except that the fraction of down-scattered events was measured to be only 3% compared with up to 60% for the flood source. For the  $^{99m}\text{Tc}/^{99m}\text{Tc}$  study,

9.5% of the emission image was subtracted from the transmission image (after first smoothing the emission image with a  $3 \times 3$  kernel) to compensate for the fraction of emission counts contributing to the 7 pixel wide electronic window. For the  $^{201}\text{Tl}/^{153}\text{Gd}$  study, down scatter from the upper peak of  $^{201}\text{Tl}$  into the  $^{153}\text{Gd}$  window was found to be negligible and was ignored. Similarly, down scatter from the  $^{153}\text{Gd}$  window into the lower  $^{201}\text{Tl}$  emission window was found to be negligible.

After performing crossover corrections, emission studies were scatter corrected using a transmission dependent convolution subtraction method (13). These data were prefiltered using a Butterworth two-dimensional filter of order 4 and cut-off frequency equal to half the Nyquist frequency and reconstructed using a ramp filter cut-off at the Nyquist frequency. Attenuation images were formed by reconstructing the natural logarithm of blank-to-transmission ratios using a Shepp-Logan filter with roll-off at the Nyquist frequency. For the situations where emission and transmission radionuclides were different, reconstructed  $\mu$  values were scaled to compensate for the difference in energies using experimentally derived scalars. The scaling of  $\mu$  values has been shown to be reasonably linear in this energy range (18).

The attenuation reconstructions were then used in a two-step procedure to correct the emission images for attenuation (21). The attenuation correction is a hybrid of the Chang (1) and Morozumi (4) algorithms. Briefly, the Chang method for deriving a matrix of attenuation correction factors (i.e., the average attenuation over all projections to each point in the reconstructed matrix) is calculated and multiplied by the uncorrected emission reconstruction to give a first estimate of an attenuation corrected reconstruction. The second step is to forward project this reconstruction twice, with and without attenuation, to give synthetic projections "in air" (i.e., without attenuation) and in the subject. The ratio of these two sets of projections provides attenuation correction factors which are then applied to the original acquired data prior to backprojection. While this second step can be repeated iteratively, in our experience only one iteration is required using measured attenuation data.

### Human Studies

Finally, two studies were performed on human subjects. In the first study a lung perfusion scan was acquired on a normal, healthy 49-yr-old female volunteer following intravenous administration of  $^{99\text{m}}\text{Tc}$ -MAA. The study was approved by the hospital ethics committee and informed consent was obtained. The aim of the study was to compare the separate measurement of emission and transmission distributions with a simultaneous acquisition. In each case, data were acquired at 64 angles using a  $360^\circ$  orbit. Acquisition times were adjusted so that the total counts in each study were approximately the same, allowing for radionuclide decay and the increase in scanning time when using the line source. Consequently, the separate emission and transmission studies were acquired for 15 sec at each projection, while the simultaneous study was 17 sec per projection. The line source was filled with 6 GBq of  $^{99\text{m}}\text{Tc}$ . A blank scan was acquired for 20 sec per projection prior to the subject studies. In subsequent processing, all scans were corrected for difference in acquisition times and decay of the radionuclide. Both separate and simultaneous studies were prefiltered using a Butterworth two-dimensional filter of order 4 and critical frequency equal to half the Nyquist frequency. The studies were then reconstructed using a ramp filter cut-off at the Nyquist frequency, with and without corrections for scatter and attenuation (21).

**TABLE 1**  
Uniformity Measurements Using  $^{57}\text{Co}$  Sheet Source and Collimated  $^{153}\text{Gd}$  Line Source

Method*	Uniformity index	Integral uniformity	Differential uniformity
$^{57}\text{Co}$ separate	4.8	5.0%	3.5%
$^{57}\text{Co}$ simultaneous	6.8	5.9%	3.8%
$^{153}\text{Gd}$ planar	10.5	19.9%	8.1%
$^{153}\text{Gd}$ SPECT	10.0	20.1%	8.1%

\*The  $^{57}\text{Co}$  sheet source measurements indicate gamma camera performance with and without the presence of the line source operating in simultaneous mode. The  $^{153}\text{Gd}$  line source measurements indicate uniformity of the line source itself during static (planar) and rotating (SPECT) acquisitions.

A further study was acquired on a patient undergoing a routine  $^{201}\text{Tl}$  myocardial perfusion rest-redistribution protocol. The aim of this study was to examine the feasibility of using simultaneously acquired emission and transmission data to perform attenuation correction in one of the most commonly performed nuclear medicine applications. A simultaneous study was acquired with  $^{153}\text{Gd}$  as the transmission source 4 hr after the administration of 120 MBq of  $^{201}\text{Tl}$ . Data were acquired at 64 angles, using a  $360^\circ$  orbit and 20 sec per angle. The emission data were prefiltered using a Metz two-dimensional image-dependent filter (22). No scatter correction was applied as this has not been fully validated for use with  $^{201}\text{Tl}$ . The data were reconstructed using a ramp filter cut-off at the Nyquist frequency with and without attenuation correction using the simultaneously acquired transmission data (21).

## RESULTS

### Line Spread Function

The measured line spread function in air of the line source had a full width at half maximum (FWHM) of 14.5 mm and a full width at tenth maximum (FWTM) of 21.1 mm when used with a LEGP collimator. When measuring transmission through 10 cm of tissue-equivalent material, the FWHM was 14.6 mm and the FWTM was again 21.0 mm, indicating that most scattered photons are eliminated due to collimation of both the detector and the line source. This line spread results in 99% of the transmission flux being recorded within the 7 pixel wide ( $64 \times 64$  matrix) electronic window employed in this study and 1% of the flux falling outside the window.

### Uniformity

Uniformity figures for both the  $^{57}\text{Co}$  sheet source and the  $^{153}\text{Gd}$  line source are given in Table 1. In the LEGP collimator, some imperfections were demonstrated using the line source that were not seen with the sheet source, presumably due to the fine collimation of the line source. This is the reason attributed to the poorer uniformity figures for the line source compared with the sheet source. The defects were not evident when the collimator was changed to a low-energy, high-resolution one. Differences due to gamma camera performance at different energies were likewise discounted as the results were consistent with both  $^{99\text{m}}\text{Tc}$  and  $^{153}\text{Gd}$  line sources. These effects were constant

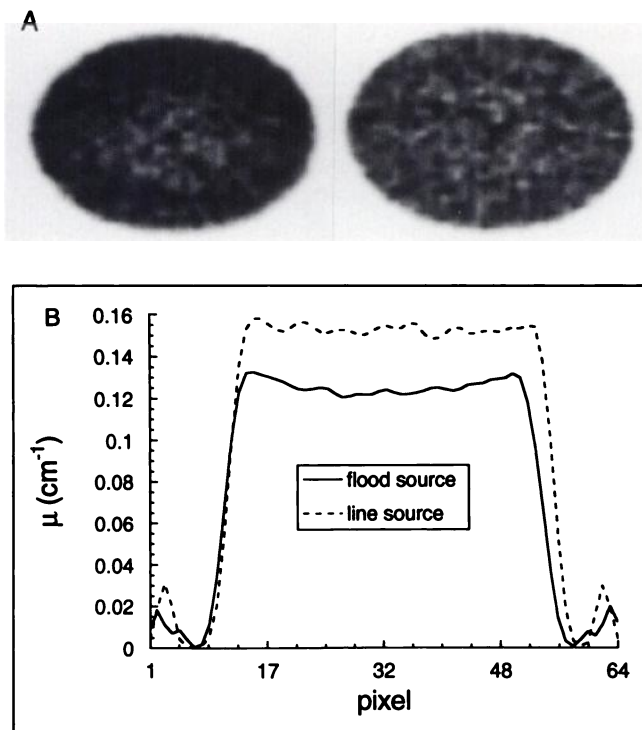


**FIGURE 5.** (A) Reconstructed attenuation images of a water-filled elliptical phantom using an uncollimated sheet source (left image) and the collimated transmission line source (right image). A reduction in attenuation values is seen towards the center of the image using the flood source due to build-up of scattered events giving rise to an apparent increase in transmitted counts. (B) Profiles through the attenuation images of (A). An appreciable dip is seen towards the center of the flood source profile, whereas the line source gives a more uniform reconstruction with values close to the expected narrow-beam attenuation coefficient for  $^{99m}\text{Tc}$  in water ( $0.15 \text{ cm}^{-1}$ ), indicating less scatter in the measurement.

with rotation angle and reinforced the need to use a blank scan for calculating the attenuation projections rather than assuming a single scalar value, as this causes nonuniformities to cancel when calculating the ratio of blank-to-transmission count rates. Any variation in velocity would degrade differential uniformity in particular, but this was not observed.

### Reconstruction of Attenuation Coefficients

A mean attenuation coefficient of  $0.15 \pm 0.01 \text{ cm}^{-1}$  was measured for the water-filled elliptical phantom using a  $^{99m}\text{Tc}$  line source. This agrees with the published value of  $0.15 \text{ cm}^{-1}$  for 140 keV photons (23) and compares with  $\mu = 0.13 \pm 0.01 \text{ cm}^{-1}$  obtained using the uncollimated flood source. The reduced attenuation coefficient in the case of the flood source is due to scattered events being recorded in the transmission images, resulting in an apparent build-up of counts (i.e., lower attenuation coefficient) towards the center of the object. This is further illustrated in Figure 5 by the decrease in the attenuation profile through the reconstructed image from the flood source study which is not seen on the line source image.

### Simultaneous Acquisition

Attenuation values and activity concentrations were determined for each of the emission-transmission radionuclide combinations and for both separate and simultaneous acquisitions. These were obtained by calculating the mean of six small ( $2.5 \text{ cm} \times 2.5 \text{ cm}$ ) ROIs in the images and the standard deviation of the means. The results are summarized in Table 2. The ROI values from the separate and simultaneous measurements were compared using a paired t-test for each of the radionuclide combinations studied. The differences did not reach significance at the  $p = 0.05$  level for either attenuation or activity values.

### Human Studies

Reconstructed attenuation and lung perfusion images are shown in Figure 6 for the separate and simultaneous cases. Qualitatively, there are no appreciable differences between the images obtained from separate measurements and those obtained simultaneously. Attenuation values obtained for the heart and lung regions were  $0.16 \pm 0.01$  and  $0.05 \pm 0.01$  respectively in both the separate and simultaneous studies. After correcting for scatter, attenuation and radioactive decay, the estimate of total counts in the lungs was 5% less in the simultaneous study than in the separate study. The simultaneous study was performed approximately 30 min after the separate study. Breakdown of the macro aggregates during this period and subsequent clearance from the lungs may partially account for the difference.

Images of myocardial perfusion using  $^{201}\text{Tl}$  reoriented parallel to the short axis of the heart are shown in Figure 7. The images in the top row were reconstructed without attenuation correction, whereas the images in the bottom row were corrected for attenuation using transmission data acquired simultaneously with the emission data. Differences between the two sets of images are mainly seen towards the base of the heart, where photon attenuation results in a relative decrease in reconstructed activity in the

**TABLE 2**  
Comparison of Reconstructions from Separate and Simultaneous Acquisitions Using the Scanning Line Source\*

Radionuclides <sup>†</sup> (Em/Tr)	Attenuation ( $\text{cm}^{-1}$ )		Emission ( $\text{ct} \cdot \text{sec}^{-1} \cdot \text{pixel}^{-1}$ )	
	Separate	Simultaneous	Separate	Simultaneous
$^{201}\text{Tl}/^{153}\text{Gd}$	$0.18 \pm 0.01$	$0.18 \pm 0.01$	$0.51 \pm 0.01$	$0.49 \pm 0.02$
$^{99m}\text{Tc}/^{99m}\text{Tc}$	$0.15 \pm 0.01$	$0.15 \pm 0.01$	$0.41 \pm 0.02$	$0.41 \pm 0.01$
$^{99m}\text{Tc}/^{153}\text{Gd}$	$0.15 \pm 0.01$	$0.15 \pm 0.01$	$0.41 \pm 0.02$	$0.40 \pm 0.02$

\*Values quoted are for the mean of six small ( $2.5 \text{ cm} \times 2.5 \text{ cm}$ ) ROIs placed on the reconstructed images and the standard deviation of the means.

<sup>†</sup>Comparisons were made using various combinations of emission (Em) and transmission (Tr) radionuclides, representing the three possible scenarios: (1) Em energy < Tr energy, (2) Em energy = Tr energy and (3) Em energy > Tr energy.

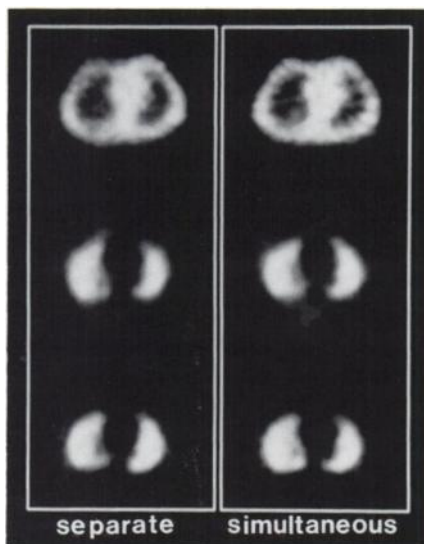


**FIGURE 6.** Reconstructed images obtained from separate (left) and simultaneous (right) acquisitions on a human volunteer undertaking a  $^{99m}\text{Tc}$ -MAA lung perfusion study. In the top row are the separately and simultaneously acquired attenuation images. The emission images in the middle row were reconstructed without correction for attenuation or scatter. The emission images in the bottom row were corrected for attenuation and scatter using the corresponding attenuation data in the top row.

inferior and infero-septal walls. This artefactual reduction is removed by attenuation correction.

## DISCUSSION

The utilization of transmission data in attenuation correction has been shown to provide improved accuracy compared with the assumption of a constant attenuation coefficient for the object (4–11). However, in the clinical environment, transmission data must be easily acquired without significantly increasing the duration of the study. The scanning line source reported in this paper is a practical method for providing this. It has been shown that it is possible to use any combination of emission and transmission radionuclide, including the situation where the same radionuclide is used for both measurements, by applying the appropriate windowing. The latter is particularly attractive for generating accurate attenuation coefficient reconstructions at the same photon energy as the emission radionuclide. An example of this is shown in Figure 6, where a simultaneous SPECT lung scan was acquired using  $^{99m}\text{Tc}$  for both the emission and transmission sources. This was not possible with previous methods using a flood source (9,14,16). While transmission measurements using  $^{99m}\text{Tc}$  are possible with our current method,  $^{153}\text{Gd}$  ( $E_\gamma = 98$  keV, 103 keV;  $T_{1/2} = 242$  days) and  $^{57}\text{Co}$  ( $E_\gamma = 122$  keV;  $T_{1/2} = 271$  days) remain useful transmission sources due to the suitability of their photon energies and radioactive half-lives. The attenuation values obtained using different radionuclides have been shown to be linearly related within the energy range used for most SPECT applications (18) and can, therefore, be scaled to appropriate values. The flexibility afforded by this approach means that transmission

measurements can be made using different radionuclides for quantitative corrections encompassing the range of SPECT studies performed in the clinical nuclear medicine department. In addition, the scan time is only slightly increased (approximately 10%), so that quantitative measurements can be made without seriously affecting patient throughput. A further advantage of the scanning line source is the reduction in scattered photons in the transmission measurement, as indicated by the agreement between measured attenuation coefficients and published narrow-beam values. Application of narrow-beam attenuation values is particularly important when applying attenuation correction to emission data that has been corrected for scatter.

Alternative geometries for transmission tomography have been suggested which also yield narrow-beam measures, including the use of a point source at the focus of a cone-beam collimator (24). Converging geometry when combined with multidetector SPECT systems also enables emission and transmission data to be acquired simultaneously (25,26). A disadvantage of this method, however, is that the transmission data are truncated due to the restricted field of view, leading to possible inaccuracies in attenuation correction. Different strategies using iterative reconstructions have been implemented to address this problem, however, and it would not appear to be a major limitation (27,28). As the scanning line source uses parallel-hole collimation, this problem does not need to be addressed.

Iterative reconstruction techniques, i.e., expectation maximization (EM) (29), could be used for both emission and attenuation reconstructions described in this work (30), and would be likely to improve the signal-to-noise ratio in both sets of data. However, they are still generally unavailable on most commercial systems, whereas filtered-backprojection is ubiquitous. An important feature of this work is that it is generally applicable on existing systems

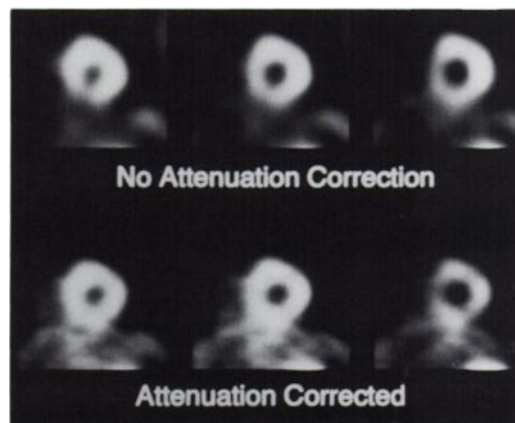


**FIGURE 7.** Short axis reconstructions of a clinical  $^{201}\text{Tl}$  myocardial perfusion study using simultaneous acquisition of emission and transmission data. The images on the top row have been reconstructed without attenuation correction. The images on the bottom row have been corrected for photon attenuation using the simultaneously acquired transmission data.

with little modification. Acceleration of the EM algorithm has been a subject of investigation in our department, again with an emphasis on practicality. A modification of EM has been developed which uses subsets of the projections during each iteration, rather than the full dataset, resulting in an order of magnitude reduction in reconstruction time (31). This may be a practical alternative to methods based on filtered backprojection.

The scanning transmission line source is currently being used in a clinical trial to assess the utility of scatter and attenuation correction schemes as well as the simultaneous emission-transmission technique. The clinical trial will involve studies of the thorax, such as myocardial perfusion imaging, as these present the most challenging situation for accurate quantification due to the inhomogeneity of tissue densities. Further improvements in the design of the device are also being investigated, including the implementation of the electronic circuitry as a single plug-in board suitable for an inexpensive IBM PC (or compatible), and optimizing the collimation to make more efficient use of the available transmission source photon flux.

Improvements in SPECT detector and collimator design have produced devices of higher resolution and greater sensitivity utilizing multidetector and other novel approaches (32,33). While these devices produce qualitatively impressive scans, they have neglected the potential to further improve the quantitative accuracy of SPECT data. For this, attenuation and scatter correction are essential. As outlined above, methods have been developed for simultaneous acquisition of emission and transmission data on triple-head SPECT systems (25,26). Although the scanning line source has been designed for use with single-head cameras, it is also possible to implement the method on dual or triple-head cameras with adjacent detectors oriented at 90 degrees to each other. It is, therefore, suggested that future developments in detector design seek to incorporate transmission measurements into the system.

## CONCLUSIONS

This paper presents a collimated scanning transmission line source which yields accurate measures of a narrow-beam attenuation coefficient of the object under investigation simultaneous with the measurement of emission photons. The transmission acquisition data are no longer severely corrupted by cross-talk from the higher energy emission photons scattered into the transmission photopeak because the technique uses a combination of physical and electronic collimation to separate the emission and transmission data. As a consequence of this approach, there is far greater flexibility in the combinations of transmission and emission nuclides which may be utilized. The same radionuclide can be used for transmission and emission with only a minimal increase in acquisition time. The line source also provides better shielding, thus reducing radiation exposure to staff. Most importantly, this technique allows transmission measurements, desirable for

quantitative accuracy, to be acquired in a practical time frame, which is essential if SPECT is to be used as a quantitative imaging tool in a clinical nuclear medicine department.

## ACKNOWLEDGMENTS

The authors thank Peter Cook, Patrick Hooper, Peter Farleigh, Adam Osiecki and Karol Wollen for their contributions; the Australian Nuclear Science and Technology Organisation (ANSTO) who aided in the design of the line source collimation and in supplying  $^{153}\text{Gd}$ ; and Nuclear Fields Pty Ltd., Sydney, for providing the materials and manufacturing the prototype scanning line source. This work was supported by a grant from the National Health and Medical Research Council (Australia).

## REFERENCES

1. Chang LT. A method for attenuation correction in radionuclide computed tomography. *IEEE Trans Nucl Sci* 1978;25:638-643.
2. Moore SC. Attenuation compensation. In: Ell P, Holman B, eds. *Computed emission tomography*. London: Oxford University Press; 1982:339-360.
3. Gullberg GT, Huesman RH, Malko JA, Pelc NJ, Budinger TF. An attenuated projector-backprojector for iterative SPECT reconstruction. *Phys Med Biol* 1985;30:799-816.
4. Morozumi T, Nakajima M, Ogawa K, Yuta S. Attenuation correction methods using the information of attenuation distribution for single photon emission CT. *Med Imag Tech* 1984;2:20-28.
5. Bailey DL, Hutton BF, Walker PJ. Toward quantitation in SPECT: a dual radionuclide method for accurate attenuation correction. *Aust NZ J Med* 1985;15:576.
6. Malko JA, van Heertum RL, Gullberg GT, Kowalsky WP. SPECT liver imaging using an iterative attenuation correction algorithm and an external flood source. *J Nucl Med* 1986;27:701-705.
7. Manglos SH, Jaszczak RJ, Floyd CE, Hahn LJ, Greer KL, Coleman RJ. Nonisotropic attenuation in SPECT: phantom tests of quantitative effects and compensation techniques. *J Nucl Med* 1987;28:1584-1591.
8. Murase K, Itoh H, Mogami H, et al. A comparative study of attenuation correction algorithms in single photon emission computed tomography (SPECT). *Eur J Nucl Med* 1987;13:55-62.
9. Tsui BM, Gullberg GT, Edgerton ER, et al. Correction of nonuniform attenuation in cardiac SPECT imaging. *J Nucl Med* 1989;30:497-507.
10. Ljungberg M, Strand S-E. Attenuation correction in SPECT based on transmission studies and Monte Carlo simulations of build-up functions. *J Nucl Med* 1990;31:493-500.
11. Galt JR, Cullom SJ, Garcia EV. SPECT quantification: a simplified method of attenuation and scatter correction for cardiac imaging. *J Nucl Med* 1992;33:2232-2237.
12. Ljungberg M, Strand S-E. Scatter and attenuation correction in SPECT using density maps and Monte Carlo simulated scatter functions. *J Nucl Med* 1990;31:1560-1567.
13. Meikle SR, Hutton BF, Bailey DL, Fulton RR, Schindhelm K. SPECT scatter correction in nonhomogeneous media. In: Colchester ACF, Hawkes DJ, eds. *Information processing in medical imaging, 12th international conference*. Berlin: Springer-Verlag; 1991:34-44.
14. Bailey DL, Hutton BF, Walker PJ. Improved SPECT using simultaneous emission and transmission tomography. *J Nucl Med* 1987;28:844-851.
15. Murphy P. Quantitative emission tomography [Editorial]. *J Nucl Med* 1987; 28:922-923.
16. Frey EC, Tsui BMW, Perry JR. Simultaneous acquisition of emission and transmission data for improved thallium-201 cardiac SPECT imaging using a technetium-99m transmission source. *J Nucl Med* 1992;33:2238-2245.
17. Vanregemorter J, DeConinck F. One phantom providing a complete set of tests [Abstract]. *J Nucl Med* 1987;26:33.
18. Bailey DL, Hutton BF. Simultaneous emission and transmission tomography. *Proceedings of 10th International conference on information processing in medical imaging*. Utrecht 1988; 559-575.
19. NEMA. Performance measurements of scintillation cameras. *National Electrical Manufacturers Association*. Washington, DC 1980; NU-1-1980.
20. Cox NJ, Diffey BJ. A numerical index of gamma-camera uniformity. *Br J Radiol* 1976;49:734-735.
21. Bailey DL, Meikle SR, Eberl S, Fulton RR, Hooper PK, Hutton BF. A



- quantitative SPECT regime. *Proceedings of IEEE Medical Imaging Conference, volume 2*. Orlando, 1992:1005-1007.
22. King MA, Penney BC, Glick SJ. An image-dependent Metz filter for nuclear medicine images. *J Nucl Med* 1989;29:1980-1989.
  23. Hubbell JH. Photon cross sections, attenuation coefficients and energy absorption coefficients from 10 keV to 100 GeV. *National Bureau of Standards*. U.S. Department of Commerce 1969; NSRDS-NBS 29.
  24. Manglos SH, Bassano DA, Duxbury CE, Capone RB. Attenuation maps for SPECT determined using cone beam transmission computed tomography. *IEEE Trans Nucl Sci* 1990;37:600-608.
  25. Gullberg GT, Tung C-H, Zeng GL, Christian PE, Datz FL, Morgan HT. Simultaneous transmission and emission computed tomography using a three-detector SPECT system [Abstract]. *J Nucl Med* 1992;33:901.
  26. Tung C-H, Gullberg GT, Zeng GL, Christian PE, Datz FL, Morgan HT. Nonuniform attenuation correction using simultaneous transmission and emission converging tomography. *IEEE Trans Nucl Sci* 1992;39:1134-1143.
  27. Gullberg GT, Zeng GL, Datz FL, Christian PE, Tung C-H, Morgan HT. Review of convergent beam tomography in single photon emission computed tomography. *Phys Med Biol* 1992;37:507-534.
  28. Manglos SH. Truncation artifact suppression in cone-beam radionuclide transmission CT using maximum likelihood techniques: evaluation with human subjects. *Phys Med Biol* 1992;37:549-562.
  29. Shepp LA, Vardi Y. Maximum likelihood reconstruction for emission tomography. *IEEE Trans Med Imag* 1982;MI-1:113-122.
  30. Lang K, Carson R. EM reconstruction algorithms for emission and transmission tomography. *J Comput Assist Tomogr* 1984;8:306-316.
  31. Hudson MH, Hutton BF, Larkin R. Accelerated EM reconstruction using ordered subsets [Abstract]. *J Nucl Med* 1992;33:960.
  32. Genna S, Smith AP. The development of ASPECT, an angular single crystal brain camera for high efficiency SPECT. *IEEE Trans Nucl Sci* 1988;35:654-658.
  33. Lim CB, Walker R, Pinkstaff C, et al. Triangular SPECT system for three-dimensional total organ volume imaging: design concept and preliminary imaging results. *IEEE Trans Nucl Sci* 1985;32:741-747.